A pseudopotential density functional theory study of native defects and boron impurities in FeAl



2006 J. Phys.: Condens. Matter 18 8859

(http://iopscience.iop.org/0953-8984/18/39/016)

INSTITUTE OF PHYSICS PUBLISHING JOURNAL OF PHYSICS: CONDENSED MATTER

J. Phys.: Condens. Matter **18** (2006) 8859–8876 doi:10.1088/0953-8984/18/39/016

# A pseudopotential density functional theory study of native defects and boron impurities in FeAl

**C D Latham[1,2], S Öberg[1], P R Briddon[3] and F Louchet[4]**

[1] Institutionen för matematik, Luleå Tekniska Universitet, SE-97187 Luleå, Sweden
[2] Sähkökekniikan osasto, Lappeenrannan Teknillinen yliopisto, PL 20, FIN-53851 Lappeenranta, Finland
[3] Physics Centre, School of Natural Science, University of Newcastle upon Tyne, Newcastle, NE1 7RU, UK
[4] LGGE, 54 rue Molière, BP 96—Domaine Universitaire, F-38402 Saint Martin d'Hères, France

E-mail: latham@math.ltu.se

Received 17 February 2006, in final form 19 July 2006
Published 15 September 2006
Online at stacks.iop.org/JPhysCM/18/8859

**Abstract**

The structures and energies of point defects and point defect complexes in $B2$ iron aluminium FeAl are calculated using a local density functional theory based method with large supercells. Particular emphasis is given to pseudopotential quality, choice of chemical potentials used to calculate defect formation energies, and how these are affected by magnetism. Both purely native defects and those containing boron atoms are considered. It is found that the relative stabilities of isolated point defects versus defect complexes depends on whether the material contains excess iron or aluminium. The situation in material containing boron is further complicated by the existence of iron borides in more than one form. We propose that the interaction between point defects, dislocations, and antiphase boundaries, where the local atomic environment has some similarities with antisite defects, also depends on the alloy composition. It is likely that these interactions are part of the underlying mechanism responsible for the unusual mechanical properties of iron aluminides.

## 1. Introduction

It is well known that the concentration of certain point defects (vacancies, interstitials, impurities, etc) affect the behaviour of dislocations in crystals, and hence their mechanical properties. In general terms, the formation energies of these defects depend on the chemical potentials of a system. For an alloy, this may be controlled by its composition. The work presented in this paper is a study of point defects and defect complexes in iron aluminium (FeAl) with the eventual aim of better understanding the mechanical properties of this material.

FeAl is an ordered intermetallic compound that crystallizes in the $B2$ or $P\bar{3}m$ simple cubic structure, similar to CsCl. Its structure is in effect that of bcc iron with every other atom

  

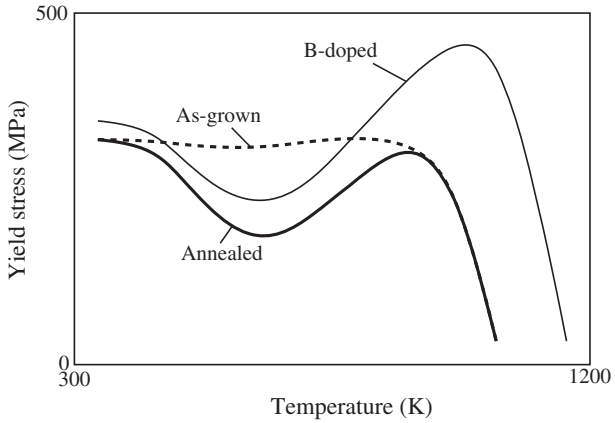


**Figure 1.** Schematic illustration of the yield stress of $B2$-FeAl as a function of temperature.

replaced by aluminium. Consequently, its density is only $\approx$73% of that for bcc-Fe. The material is also very hard and corrosion resistant. $B2$-FeAl belongs to a group of materials (mostly ordered intermetallic compounds, but also a few ceramics) that exhibit unusual behaviour in terms of their yield stress as a function of temperature. Unlike most materials which become softer with increasing temperature, over a finite range $B2$-FeAl becomes much stronger, rising to a maximum at about 800–1000 K. Materials of this type also have a small strain rate sensitivity and a large work hardening rate in this temperature range. Adding small quantities of boron of $\sim$100–400 ppm to $B2$-FeAl increases its peak strength by up to 50%, and raises the temperature at which the peak occurs by $\sim$100 K [1, 2]. This is illustrated in figure 1. Furthermore, internal friction studies reveal complex behaviour in Fe–Al alloys, and provide detailed information about the effects of temperature, ternary additions, mechanical and thermal history, etc [3]. This is a rich subject, where there exists a large body of experimental observations, yet the underlying mechanisms at a fundamental level often remain unknown.

Several models to explain stress anomalies, mostly for $\beta$-CuZn, have been proposed. These need to take into account three key observations. Firstly, in single crystals the magnitude of the stress anomaly is anisotropic. This suggests that the role of cross-slip may be important. The second, and possibly most crucial observation, is that the predominant slip system changes at the temperatures where the peak yield stress occurs. In $B2$-structure materials these have a $\langle 111 \rangle$ slip direction below the stress peak temperature, and $\langle 100 \rangle$ or sometimes $\langle 110 \rangle$ type above. The $\langle 111 \rangle$ dislocations are dissociated into two $1/2\langle 111 \rangle$ superpartial dislocations separated by an antiphase boundary (APB). Finally, it is observed that the temperature of the stress peak increases with strain rate. This implies that the slip process above the peak is a normal thermally activated one, while the one below is not.

Another factor that has been correlated with the unusual mechanical properties of FeAl is the presence of vacancies [4–7]. However, the vacancy-hardening model that is proposed explains neither the anisotropy of the stress anomaly nor the small strain rate sensitivity. Instead, a more successful model is based on the idea that $\langle 111 \rangle$ superdislocations dissociate into $\langle 100 \rangle + \langle 110 \rangle$ ordinary ones with low mobility. Moreover, the dissociation process is thermally activated, and hence in the anomalous regime the superdislocations remain locked [8, 9]. These models are discussed in a review by Morris and Muñoz-Morris; however, a number of unanswered questions remain that are highlighted by the authors [10].

Some further clues about the origin of the stress anomaly and vacancy-hardening mechanism are provided by electron microscopy observations of specimens under strain

*in situ* [2]. According to this, the leading superpartial dislocation undergoes localized climb at points where vacancies are encountered. When the trailing superpartial subsequently passes these points, annihilation of the trailing APB does not occur. APB tubes are thus formed in the wake of the superpartial, increasing the drag force, until so many tubes have accumulated that movement ceases. An increase in stress is then required, in order to enhance multiplication and balance the loss of these immobilized dislocations. At temperatures above the yield stress maximum, ⟨100⟩ dislocations are more mobile than ⟨111⟩ superdislocations and normal behaviour resumes. It is thought that boron segregates at ⟨110⟩ edges, and thus interferes with the high-temperature deformation mechanism involving ⟨100⟩ and ⟨110⟩ glide, hence raising the temperature at which the yield stress peak occurs. However, the exact details of the mechanism are unknown.

The subject has received considerable attention from theorists. Calculations based on density functional theory (DFT) and the local-density approximation (LDA) have mainly focused on two aspects of the system.

The first concerns the contribution of the exchange–correlation energy term $E_{ex}$ to the total energy, and magnetic effects. Stoichiometric $B2$-FeAl is a paramagnetic compound; however, calculations based on the local-spin-density approximation (LSDA) for $E_{ex}$ predict that the ground state is ferromagnetic [11–14]. The generalized gradient approximation (GGA) yields similar results. In the case of $Fe_3Al$, the GGA predicts that the $L1_2$ structure has lower energy than the experimentally observed $D0_3$ phase, while the LSDA gives the correct ordering [15]. This is made more puzzling by the fact that calculations based on the LSDA predict incorrectly that the energy per atom of fcc-Fe is about 0.08 eV lower than ferromagnetic bcc-Fe [16], while the GGA gives the correct ordering [17, 18]. These energy differences are relatively small, and quite possibly the truth is that both approximations are insufficiently reliable to resolve them. Moreover, in the case of Fe–Al alloys, their unusual electronic structure is thought to exacerbate the well-known slight overstabilization of higher spin states from which the LSDA and GGA suffer [19–21]. One approach for correcting this problem is to introduce a non-local screened Coulomb potential $U$ into the expression for $E_{ex}$ [21, 22]. The difficulty with this LDA + $U$ method lies in determining the parameter $U$. In practice, it is adjusted for each system to reproduce the experimentally observed results [19].

Structural disorder also affects the magnetic behaviour. One theoretical interpretation of experimental results concludes that there is a delicate balance between ferromagnetic and antiferromagnetic ordering [23, 24]. In the $B2$ structure, Fe atoms only induce ferromagnetism when they are nearest neighbours (such as in antisite defects, for example). Otherwise, they have an indirect antiferromagnetic interaction via an intermediate Al atom. Ferromagnetism is also enhanced at the expense of lower magnetic symmetries in small clusters, according to other calculations [25]. According to another point of view, ideal, perfectly ordered FeAl has a ferromagnetic ground state, while the material is paramagnetic when structural, thermal, and magnetic disorder are properly taken into account [26].

The second type of calculation, based on a combination of DFT and statistical mechanics, is used to estimate formation energies, concentrations, and structures of native point defects and defect complexes, and isolated impurity atoms [27–33]. The effect of using different approximations for $E_{ex}$ on point defect formation energies is also considered in the last of these studies. Similar methods are also used in a computational study of the Ni–Fe–Al system [34]. The results reported in [27–30] are based on what are now considered rather small model systems constructed in supercells of 16 or 32 atomic sites. The effective defect concentration is these models is very high, such that in a supercell formalism defects may interact significantly with their images. The more recent results reported in [31–33] are based on supercells containing 54 atomic sites. At this size, the interaction between point defects and

their images is probably acceptable. Nevertheless, results for larger supercells are desirable. Among these calculations, only [33] reports defect energies for boron impurities, and then only as isolated boron. Information about defect complexes is lacking, yet these almost certainly play an important role in the mechanical properties of FeAl and related materials.

## 2. Method

### *2.1. Total energy calculations*

The total energies of supercells are calculated using a method based on self-consistent local-density-functional theory, AIMPRO. Only a brief summary of the main points is given here: for a more detailed description, see [35, 36].

The exchange–correlation energy contribution is evaluated according to the formula described by Perdew and Wang [37]. A basis set of Gaussian orbitals is used to describe the Kohn–Sham wavefunctions of the valence electrons. Suitable multiplicative factors provide *s*-, *p*- and, optionally for each exponent, *d*-orbital symmetries. Even-tempered basis sets are generated and optimized by a similar procedure to that described in previous work [38]. Core electrons are replaced by norm-conserving pseudopotentials based on the Troullier–Martins (TM) scheme [39]. This is modified by a nonlinear core correction (nlcc) to include approximately the effects of the Fe core electrons without explicitly including them in the valence orbitals [40]. The charge density is represented by a plane-wave basis in reciprocal space. An automatic procedure ensures that the number of shells of vectors $\boldsymbol{R}_L$ used to evaluate the Madelung energy is sufficient.

The forces acting on each atom are given by an analytical formula derived from the total energy expression. Structural optimization to minimize the total energy is performed by a conjugate-gradient algorithm. Defects are constructed in supercells with cubic crystal symmetry, where the ideal $B2$-FeAl structure contains 54 or 128 atoms. The lattice parameters describing supercells are those that minimize $E_{\text{total}}$ for pure $B2$-FeAl; these are normally held fixed during the energy minimization procedure.

We use the Monkhorst–Pack (MP) scheme to sample the band structure [41]. Both the largest reciprocal lattice vector of the charge–density Fourier expansion and the mesh of $\boldsymbol{k}$-points are chosen so that the total energy $E_{\text{total}}$ is converged with respect to these parameters. Proper account is taken of the band-structure for the occupancies of each Kohn–Sham level. The states are filled according to a Fermi function with a small, finite temperature that is chosen to improve the numerical stability of the self-consistency procedure. A correction is applied to $E_{\text{total}}$ to account for the entropy that this introduces.

In supercells containing 54 atomic sites, MP-4 $\times$ 4 $\times$ 4 $\boldsymbol{k}$-point sampling is sufficient for structural relaxation. However, to achieve full convergence in $E_{\text{total}}$ to the level $\epsilon \lesssim 10^{-4}$ Hartrees or about 3 meV per FeAl, it is necessary to use MP-8 $\times$ 8 $\times$ 8 sampling. Denser grids (tested up to MP-12 $\times$ 12 $\times$ 12) give equal energies to this level of accuracy. In the highest symmetry case, MP-8 $\times$ 8 $\times$ 8 sampling leads to 20 irreducible $\boldsymbol{k}$-points. However, if a supercell of this size contains a defect posessing low symmetry, the number of $\boldsymbol{k}$-points expands to 256. The situation turns out to be very much better in supercells containing 128 atomic sites. Here, MP-2 $\times$ 2 $\times$ 2 sampling is sufficient. This has only one irreducible $\boldsymbol{k}$-point in the highest symmetry case, and at worst unfolds to only four $\boldsymbol{k}$-points. In terms of computational cost, therefore, it turns out that the smaller number of $\boldsymbol{k}$-points needed for the larger supercell partially compensates the fact that it contains more atoms. This facilitates using large supercells to validate results obtained in smaller supercells, both for our work, and that of others.

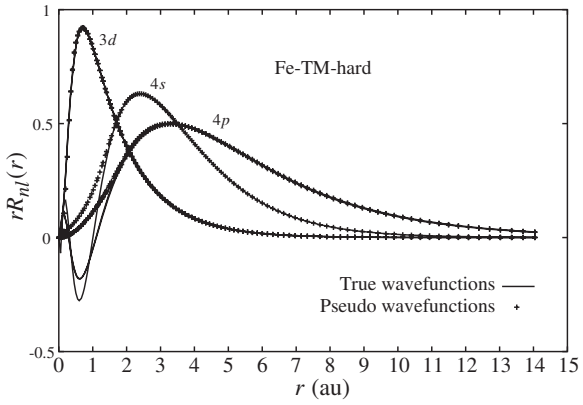


**Figure 2.** 'Hard' pseudopotential for iron where $r_{cd} = 0.65$ au $\approx 0.9 r_{\max}(3d)$.

### *2.2. Pseudopotentials*

In order to establish a reasonable balance between speed and reliability for the calculations, several pseudopotentials and many basis sets have been constructed and tested. For Al and B atoms, the optimum basis is found to be four Gaussian exponents per orbital with $d$-functions for the two smallest exponents in the basis set. Iron presents a considerably greater challenge, owing to the small radius for the peak in its $3d$ wavefunction at $r_{\max}(3d) = 0.72$ au. According to the conventional prescription for generating Troullier–Martins pseudopotentials, the radial cutoff $r_{cl}$ for each wavefunction with angular momentum $l$ should be about $0.9 r_{\max}$. This then determines the kinetic energy cutoff $E_{\text{cut}}$ needed for the *charge–density* plane-wave basis that is necessary to achieve convergence for $E_{\text{total}}$ better than the required level $\epsilon$, and hence is directly related to the computational cost[4]. Using $r_{cd} = 0.65$ au to construct a pseudopotential for Fe atoms that we label Fe-TM-hard (illustrated in figure 2), and $\epsilon \lesssim 10^{-4}$ Hartrees per FeAl, leads to $E_{\text{cut}} \approx 400$ Hartrees, or about 11 keV. This is an enormous value. If instead $r_{cd} = r_{cs} = 2.0$ au, we arrive at a large but much more economical figure of $E_{\text{cut}} \approx 150$ Hartrees while maintaining the same energy convergence criterion. This pseudopotential, labelled Fe-TM-soft, is illustrated in figure 3. A consequence of this compromise is that the pseudo-wavefunction below the cutoff radius departs very noticeably from the true wavefunction, however, it might be justified on the grounds that the main part of chemical bonding effects occur in hybridized orbitals at distances from the nuclei of atoms of around half the bond length in any material, or about 2.3 au in FeAl.

The optimum basis for the Fe pseudopotentials have five Gaussian exponents per orbital for the 'hard' one and four for the 'soft' one, leading to further savings in computational cost for the latter. Functions of $s$-, $p$-, and $d$-symmetry are applied to all exponents. Larger basis sets cause problems with numerical stability, while smaller ones are insufficient to recover the true total energies that an ideal, exact method would give.

Naturally, the 'hard' Fe pseudopotential (Fe-TM-hard) is expected to be more accurate than the 'soft' pseudopotential (Fe-TM-soft). Thus, a strategy that allows us to take advantage of the benefits that each provide is to first optimize structures in calculations with Fe-TM-soft, then substitute Fe-TM-hard and re-optimize the structure. This reduces considerably the computational effort over using only the 'hard' pseudopotential from the beginning, in addition to providing information about the relative accuracy of Fe-TM-soft.

[4] In other calculations where both the wavefunction and charge–density are expanded as plane waves, $E_{\text{cut}}$ usually refers to the wavefunction basis. The equivalent value of $E_{\text{cut}}$ for the charge–density, used here, is four times larger.

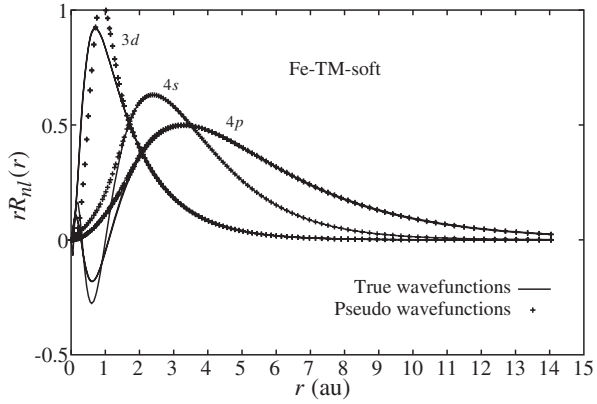


**Figure 3.** 'Soft' pseudopotential for iron where $r_{cd} = r_{cs} = 2.0$ au. Note that the fit to the Fe-3*d* wavefunction is poor in the vicinity of its peak.

### *2.3. Chemical potentials and defect formation energies*

Formation energies of defects are calculated by the conventional method, as described by previous authors [42–46]. In general terms, this is defined as,

$$E_f(q) = E_d(q) + q\mu_e - \sum_i n_i\mu_i, \tag{1}$$

where $E_f(q)$ is the formation energy of a defect in charge state $q$, and $E_d(q)$ is the total energy of a supercell containing a defect that is composed from $n_i$ atoms, molecules or formula units of type $i$ each having chemical potential $\mu_i$. The chemical potential of $i$ is defined to be the Gibbs free energy per particle. For condensed matter at zero temperature and pressure, the entropy and pressure contributions to the Gibbs free energy can be neglected. Hence, $\mu_i$ is the total energy per species. The quantity $\mu_e$ is the electron chemical potential with respect to the top of the valence band of the pure material. Since we are dealing with a metal, the term $q\mu_e = 0$.

Chemical potentials are normally subject to several restrictions, and usually chosen in a way that is appropriate to the system under consideration. For the Fe–Al system, the chemical potentials $\mu_{Al}$ and $\mu_{Fe}$ depend on whether an excess of aluminium or iron is present when the crystal is formed; hence fcc-Al metal, bcc-Fe metal, and $B2$-FeAl are the three relevant reference states that define $\mu_{Al}$, $\mu_{Fe}$, and $\mu_{FeAl}$. For the system to be in equilibrium, $\mu_{Fe}+\mu_{Al} = \mu_{FeAl}$, and it is subject to the boundary conditions, $\mu_{Fe} \leqslant \mu_{bcc\text{-}Fe}$, and $\mu_{Al} \leqslant \mu_{fcc\text{-}Al}$. The chemical potentials $\mu_{Al}$ and $\mu_{Fe}$ are thus restricted to a range determined by the heat of formation of FeAl from the elements in their standard states, $\Delta H_f = \mu_{Al} + \mu_{Fe} - \mu_{FeAl}$. In other words, this is the energy cost for the reaction Fe(s) + Al(s) $\rightarrow$ FeAl(s) at 0 K, and where a negative value means it is exothermic.

The chemical potentials for impurity atoms are usually determined by the relevant stable states that limit the solubility of the impurity. In the case of boron in Fe–Al alloys and compounds, the states that define $\mu_B$ are orthorhombic-FeB (space group $Pnma$, 62) and tetragonal-$Fe_2B$ (space group $I4/mcm$, 140). The atomic coordinates of FeB and $Fe_2B$ are described in the appendix. Both materials are ferromagnetic. The chemical potentials of B atoms in both phases are similar, but the stoichiometry is different, hence both must be taken into account when calculating the formation energies of defects containing boron along with whether the system is Fe-rich or Al-rich. Thus, the chemical potential for B atoms is determined

by either $\mu_{Fe} + \mu_B = \mu_{FeB}$ or $2\mu_{Fe} + \mu_B = \mu_{Fe_2B}$. There are also two known crystalline forms of $Fe_3B$ and numerous glassy phases of various compositions, but these are all metastable.

Individual defects can combine to form complexes. Whether this happens depends on a number of factors. First, we must assume that at least one of the components of a complex is sufficiently mobile for the constituents to encounter one another, and that both isolated entities exist in significant concentrations. If this is the case, and the complex is energetically bound with respect to the formation energies of the isolated parts, then this alone does not mean that the complex will form in significant concentrations. In equilibrium conditions, the complex made from two parts must have a formation energy that is less than the formation energies of both the components. In other words, the binding energy of the components needs to be greater than the larger of the formation energies of the two parts. However, it is commonly the case that complexes form in non-equilibrium conditions during growth and subsequent treatments. This occurs when a defect population that is created during growth at a high temperature becomes trapped or 'frozen in' upon cooling to a lower temperature. Below a certain temperature, nearly all of the component defects will condense into the complex, and cannot dissociate: the activation energy is too large to reverse the reaction.

An additional problem to consider here concerns the effects of magnetism. As explained previously, there is much uncertainty about magnetic effects in Fe–Al. We will see that, in this material, they have little effect on bulk properties; however, the opposite is true for bcc-Fe, FeB, and $Fe_2B$. Our approach in this work is to compare formation energies calculated with respect to both non-magnetic and ferromagnetic bcc-Fe, FeB, and $Fe_2B$, while using only spin-averaged total energies for both pure, ideal $B2$-FeAl and supercells containing defects. We have, in fact, attempted to calculate magnetic, spin-polarized total energies for the supercells containing model defects. Unfortunately, we are unable to achieve stable self-consistent numerical solutions to the Kohn–Sham eigenvalue problem. This is probably due to the huge total energies that norm-conserving pseudopotentials yield in comparison to the relatively small contributions from the defects. A final point to note before examining the results is that Fe–Al alloys containing more Al atoms than Fe are difficult to produce.

## 3. Results

### *3.1. Bulk properties*

A summary of values given by the AIMPRO method for the lattice parameters $a$, bulk moduli $B_0$, and pressure derivatives $B_0'$ of bcc-Fe, fcc-Al, and $B2$-FeAl, together with their observed values, is given in table 1.

Clearly, the calculated parameters for bcc-Fe are very sensitive to whether the calculation is spin-polarized or not, and to the choice of Fe pseudopotential. The lattice parameter is significantly underestimated, and the bulk modulus grossly overestimated in the spin-averaged, non-magnetic calculation. Much better agreement with experiment is found for a spin-polarized, ferromagnetic calculation. Here, the number of unpaired electrons in the calculation is optimized for each of several values of $a$ when determining the equilibrium value for $a$, and the elastic parameters $B_0$ and $B_0'$. If the magnetization $M$ is not allowed to vary with $a$, then $B_0$ is overestimated in a similar manner to the spin-averaged calculation, and $B_0'$ is ill-behaved (for most ordinary materials $B_0' \sim 4$). At the equilibrium value for $a$, the net spin magnetization is estimated to be $M \approx 2.24\ \mu_B$ using the 'soft' Fe pseudopotential and $M \approx 2.67\ \mu_B$ for the 'hard' Fe pseudopotential. The observed value is $M \approx 2.2\ \mu_B$. The spin-polarized calculations for bcc-Fe also have a significantly lower total energy per atom than spin-averaged ones. The difference when using the 'soft' Fe pseudopotential is 0.50 eV, and 1.03 eV when using the the 'hard' Fe pseudopotential.

**Table 1.** Calculated and observed lattice parameters $a$, bulk moduli $B_0$, and pressure derivatives $B_0'$ for Al, Fe, and $B2$-FeAl. Spin-averaged, non-magnetic calculations are labelled NM, and spin-polarized, ferromagnetic calculations are labelled FM.

| Description | $a$ (Å) | $B_0$ (GPa) | $B_0'$ |
|---|---|---|---|
| NM fcc-Al | 3.958 | 82.3 | 4.3 |
| *Observed* fcc-Al | 4.050 | 76 | |
| NM bcc-Fe, Fe-TM-soft | 2.741 | 313.7 | 4.6 |
| FM bcc-Fe, Fe-TM-soft | 2.813 | 219.8 | 5.0 |
| NM bcc-Fe, Fe-TM-hard | 2.690 | 324.4 | 4.5 |
| FM bcc-Fe, Fe-TM-hard | 2.814 | 198.4 | 3.5 |
| *Observed* bcc-Fe | 2.867 | 170 | |
| NM $B2$-FeAl, Fe-TM-soft | 2.825 | 203.4 | 4.1 |
| FM $B2$-FeAl, Fe-TM-soft | 2.831 | 198.1 | 4.2 |
| NM $B2$-FeAl, Fe-TM-hard | 2.800 | 206.4 | 4.2 |
| FM $B2$-FeAl, Fe-TM-hard | 2.809 | 195.0 | 4.7 |
| *Observed* $B2$-FeAl | 2.887 | 152 | |

The results for $B2$-FeAl show much less sensitivity than bcc-Fe does to whether the calculation is spin-averaged or spin-polarized, and to the choice of pseudopotential. When using the 'soft' Fe pseudopotential, the total energy per unit FeAl of the spin-polarized calculation is about 0.03 eV less than the spin-averaged case. The corresponding figure for the 'hard' Fe pseudopotential is slightly more than double this amount at 0.08 eV. The 'soft' and 'hard' Fe pseudopotentials yield values for the magnetization per unit FeAl that are $M \approx 0.72\ \mu_B$ and $M \approx 0.82\ \mu_B$, respectively.

Consequently, the value for $\Delta H_f$ given by our calculations depends on both the choice of Fe pseudopotential and on whether magnetism is included or not. In the simplest case, where elemental bcc-Fe and $B2$-FeAl are both treated as spin-averaged, non-magnetic materials, the results are $\Delta H_f = -1.20$ eV for the 'soft' Fe pseudopotential and $\Delta H_f = -1.18$ eV for the 'hard' Fe pseudopotential. From this it can be concluded that both Fe pseudopotentials appear to have similar behaviour in terms of chemical bonding, at least for bulk matertials. If spin-polarized total energies are used for bcc-Fe, while $B2$-FeAl is still constrained to be non-magnetic, then the corresponding two values for the heat of formation become $\Delta H_f = -0.71$ eV and $\Delta H_f = -0.15$ eV, respectively. The two results for the heat of formation of a fully spin-polarized, magnetic system are then $\Delta H_f = -0.74$ eV (soft) and $\Delta H_f = -0.22$ eV (hard).

Both measured and calculated values for $\Delta H_f$ reported by others vary widely. For most materials, LDA-based methods tend to give slightly overbound results for $\Delta H_f$: a similar trend is seen for $B2$-FeAl. For example, calculations in [47] by a full-potential linearized augmented Slater-type orbital method give $\Delta H_f = -0.84$ eV. The same source quotes several measured values between $-0.50$ and $-0.84$ eV. Another measurement has $\Delta H_f = -0.49 \pm 0.03$ eV [48]. Calculations by a linearized muffin-tin orbital method (self-consistent, LSDA-based) give $\Delta H_f = -1.63$ eV [20]. For a recent review of the subject, see [49].

The results presented so far provide a rough guide to the accuracy of LDA-based methods. The error in defect formation energies $E_f(q)$ when $q = 0$ is the same order of magnitude as the error in the heats of formation $\Delta H_f$ of the materials under consideration; that is typically $\sim 0.3$ eV/atom. However, when comparing the energies of different defects, the errors are generally an order of magnitude smaller, depending on the degree of cancellation of errors in $\Delta H_f$ and total energies. The error is likely to be smaller for similar configurations than for dissimilar configurations.

**Table 2.** Calculated and observed lattice parameters $a$, $b$, $c$ and structural parameters for FeB. Spin-averaged, non-magnetic calculations are labelled NM, and spin-polarized, ferromagnetic calculations are labelled FM. See the appendix for details of the four parameters $A$, $B$, $C$, and $D$ that describe the atomic coordinates.

| Description | $a$ (Å) | $b$ (Å) | $c$ (Å) | $A$ | $B$ | $C$ | $D$ |
|---|---|---|---|---|---|---|---|
| *Calculated* | | | | | | | |
| NM, Fe-TM-soft | 5.1540 | 3.0885 | 3.8603 | 0.1824 | 0.1195 | 0.0387 | 0.6200 |
| FM, Fe-TM-soft | 5.3752 | 2.9258 | 3.9641 | 0.1778 | 0.1197 | 0.0338 | 0.6177 |
| NM, Fe-TM-hard | 5.0491 | 3.0581 | 3.8112 | 0.1828 | 0.1217 | 0.0396 | 0.6226 |
| FM, Fe-TM-hard | 5.3970 | 2.8821 | 4.0133 | 0.1786 | 0.1184 | 0.0350 | 0.6141 |
| *Observed* | | | | | | | |
| Ref. [50] | 5.5047 | 2.9517 | 4.0595 | 0.1768 | 0.1194 | 0.0341 | 0.6142 |

**Table 3.** Calculated and observed lattice parameters $a$ and $c$ and structural parameter for $Fe_2B$. Spin-averaged, non-magnetic calculations are labelled NM, and spin-polarized, ferromagnetic calculations are labelled FM. See the appendix for details of the parameter $A$ that describes the positions of Fe atoms.

| Description | $a$ (Å) | $c$ (Å) | $A$ |
|---|---|---|---|
| *Calculated* | | | |
| NM, Fe-TM-soft | 4.9349 | 4.1414 | 0.1624 |
| FM, Fe-TM-soft | 5.0232 | 4.2120 | 0.1663 |
| NM, Fe-TM-hard | 4.8315 | 4.1209 | 0.1632 |
| FM, Fe-TM-hard | 5.0133 | 4.1874 | 0.1677 |
| *Observed* | | | |
| Ref. [51] | 5.107 | 4.251 | 0.1661 |

Magnetism and Fe pseudopotential quality also affect the outcome for FeB and $Fe_2B$. The spin-polarized total energy per formula unit is lower than the spin-averaged result. Using the 'soft' Fe pseudopotential, the amounts are 0.13 eV/FeB and 0.35 eV/$Fe_2B$. For the 'hard' Fe pseudopotential, these two quantities increase to 0.33 eV/FeB and 1.18 eV/$Fe_2B$. The lattice and structural parameters given by the spin-polarized calculations are nearer to their observed values than with our spin-polarization. A summary is given in tables 2 and 3.

At equilibrium, the net spin magnetizations per formula unit using the 'soft' Fe pseudopotential for FeB and $Fe_2B$ are $M = 1.16$ and 3.78 $\mu_B$, respectively. The corresponding two values obtained with the 'hard' Fe pseudopotential are $M = 2.04$ and 4.67 $\mu_B$. As with bcc-Fe, and consistent with other studies, theory tends to overestimate the observed magnetization [52]. The measured magnetization per formula unit for FeB is $M = 1.03$ $\mu_B$ [50], and for $Fe_2B$ it is $M = 3.78$ $\mu_B$ [51].

### *3.2. Vacancies*

Vacancies represent an extreme case in terms of change in volume on an atomic site. They are, therefore, a good test for whether the size of supercell used to model point defects is sufficient to accommodate properly the problem being considered. In semiconductors, vacancies are particularly complex due to electronic effects from levels in the bandgap. Although FeAl is not a semiconductor and has no bandgap, the bonding is partly covalent, and electronic effects are more important than in simpler metallic materials. Hence, vacancies also represent a severe test for pseudopotentials and basis sets.

The formation energies for aluminium vacancies $V_{Al}$ and iron vacancies $V_{Fe}$ in FeAl are presented in table 4. The values calculated by Fähnle *et al* [32] (self-consistent, mixed-

**Table 4.** Calculated formation energies $E_f$ (eV) for $V_{Al}$ and $V_{Fe}$ under Al-rich ($\mu_{Al} = \mu_{fcc\text{-}Al}$) and Fe-rich ($\mu_{Fe} = \mu_{bcc\text{-}Fe}$) conditions in $B2$-FeAl.

| Cell size | Fe pseudo-potential | Al-rich | | Fe-rich | |
|---|---|---|---|---|---|
| | | $V_{Al}$ | $V_{Fe}$ | $V_{Al}$ | $V_{Fe}$ |
| *All spin-averaged* | | | | | |
| 54 | Fe-TM-soft | 4.11 | 0.44 | 2.90 | 1.64 |
| 54 | Fe-TM-hard | 4.33 | 0.43 | 3.15 | 1.61 |
| 128 | Fe-TM-soft | 3.99 | 0.46 | 2.77 | 1.68 |
| *Spin-polarized bcc-Fe* | | | | | |
| 54 | Fe-TM-soft | 4.11 | 0.44 | 3.40 | 1.14 |
| 54 | Fe-TM-hard | 4.33 | 0.43 | 4.18 | 0.58 |
| 128 | Fe-TM-soft | 3.99 | 0.46 | 3.27 | 1.18 |
| *Other calculations* | | | | | |
| 54 | Fähnle *et al* [32] | 3.96 | 0.56 | 2.96 | 1.56 |

basis, Vanderbilt-type ultrasoft pseudopotentials, LDA) are included for comparison. From a technical viewpoint, except for the pseudopotentials, these are broadly equivalent to our spin-averaged calculations.

In all cases, $E_f$ for $V_{Fe}$ is lower than for $V_{Al}$, and lower in Al-rich material than when the system contains excess Fe. $V_{Al}$ can be excluded as a constitutional defect that accommodates non-stoichiometry in Fe-rich FeAl. The effect of supercell size is about three times greater for $V_{Al}$ than $V_{Fe}$, where the difference cannot be considered to be significant. Pseudopotential choice also has relatively little effect on $E_f$ for $V_{Fe}$ when spin-averaged, total energies are used, while it does have a moderate, noticeable effect in the case of $V_{Al}$. However, when energies for spin-polarized, ferromagnetic bcc-Fe enter into the account, $E_f$ is strongly affected by the Fe pseudopotential.

Recall that the energy contribution from magnetism in bcc-Fe is worth $\approx$0.5 eV/atom with the Fe-TM-soft pseudopotential and $\approx$1.0 eV/atom with the Fe-TM-hard pseudopotential. When the system contains excess Fe, the formation of one $V_{Fe}$ defect liberates one Fe atom from $B2$-FeAl that is 'absorbed' by the bcc-Fe reservoir; while to create one $V_{Al}$ defect costs one Fe atom from the bcc-Fe reservoir. Thus, in Fe-rich material, $E_f$ for $V_{Al}$ is higher, and $E_f$ for $V_{Fe}$ is lower, when $\mu_{Fe}$ is ferromagnetic bcc-Fe than when it is non-magnetic. Al-rich material is unaffected, as no ferromagnetic states are involved.

The difference between $V_{Al}$ and $V_{Fe}$ can further be understood by noticing that the eight atoms neighbouring the vacancy are in the first case Fe, and in the second case they are Al. The contributions to the total energy of the Fe–Al system are dominated by Fe, therefore $V_{Al}$—which involves eight times as many Fe atoms in the vicinity of the defect than $V_{Fe}$ does—is more sensitive to the size of the supercell, the choice of Fe-pseudopotential, and whether or not magnetism is included. Thus, it is important to bear this result in mind when considering defects that are centered on an Al-site, or that in some way involve several Fe atoms.

The all-spin-averaged results imply that the contribution to the total energy of vacancies from chemical bonding only is broadly similar for both Fe pseudopotentials. This means that the Fe-TM-soft pseudopotential may provide reasonable estimates of binding energies of defect complexes containing vacancies at lower computational cost than the 'hard' Fe pseudopotential involves.

Given that $V_{Fe}$ has a low formation energy, the Fe di-vacancy $(V_{Fe})_2$ complex, consisting of two $V_{Fe}$ defects on neighbouring Fe-sites in the lattice, is likely to be an important defect. For supercells with 54 atom sites, the binding energy of two isolated $V_{Fe}$ defects to form $(V_{Fe})_2$

**Table 5.** Calculated formation energies $E_f$ (eV) for $Fe_{Al}$ and $Al_{Fe}$ under Al-rich ($\mu_{Al} = \mu_{fcc\text{-}Al}$) and Fe-rich ($\mu_{Fe} = \mu_{bcc\text{-}Fe}$) conditions in $B2$-FeAl.

| Cell size | Fe pseudo-potential | Al-rich | | Fe-rich | |
|---|---|---|---|---|---|
| | | $Fe_{Al}$ | $Al_{Fe}$ | $Fe_{Al}$ | $Al_{Fe}$ |
| *All spin-averaged* | | | | | |
| 54 | Fe-TM-soft | 2.12 | −0.20 | −0.30 | 2.21 |
| 54 | Fe-TM-hard | 2.11 | −0.24 | −0.24 | 2.11 |
| 128 | Fe-TM-soft | 2.12 | −0.18 | −0.31 | 2.25 |
| *Spin-polarized bcc-Fe* | | | | | |
| 54 | Fe-TM-soft | 2.12 | −0.20 | 0.70 | 1.21 |
| 54 | Fe-TM-hard | 2.11 | −0.24 | 1.82 | 0.05 |
| 128 | Fe-TM-soft | 2.12 | −0.18 | 0.68 | 1.25 |
| *Other calculations* | | | | | |
| 54 | Fähnle *et al* [32] | 1.98 | 0.0 | 0.0 | 1.98 |

is estimated to be about 0.34 eV (Fe-TM-soft pseudopotential). In a supercell with 128 atom sites, the result is 0.31 eV. The difference in energy between these two results is not significant. Fähnle *et al* calculated the binding energy to be 0.38 eV [32].

### *3.3. Antisite defects*

The formation energies for antisite defects $Fe_{Al}$ and $Al_{Fe}$ are presented in table 5. It is again apparent from the results which only involve energies of spin-averaged calculations that chemical bonding is described equally by both Fe pseudopotentials. Under some circumstances, the formation energies of the defects are slightly negative. It is very likely that they are slightly underestimated in these cases, due to the heat of formation for FeAl being slightly overbound. Similarly, the formation energies of the complementary states are probably overestimated by about the same magnitude.

There is essentially no difference between the results for the 54-atom and 128-atom supercells. Antisites are substitutional defects where the volume change associated with them is relatively small, and the atoms neigbouring the defect remain close to their normal lattice sites, so there is nearly no long-ranged relaxation to accommodate that would make $E_f$ in the larger supercell significantly smaller.

As with vacancies, the choice of Fe pseudopotential only has a significant effect on the outcome where the total energy of spin-polarized bcc-Fe enters into the calculation. In this case, when excess Fe is present, to create $Fe_{Al}$ from its constituents has a net cost of two Fe atoms taken from bcc-Fe, while the formation of $Al_{Fe}$ liberates two Fe atoms from $B2$-FeAl that are absorbed by the bcc-Fe reservoir. Consequently, when magnetism in bcc-Fe is included in the account for antisite defects, $E_f$ changes by twice as much as it does for vacancies. When the Fe pseudopotential is Fe-TM-hard, the energy difference amounts to over 2 eV: $Fe_{Al}$ becomes a moderately high-energy defect, while $Al_{Fe}$ does the opposite. It might be concluded from this result that, contrary to expectations, $Fe_{Al}$ is not the constitutional defect that accommodates excess Fe in Fe-rich FeAl. However, we have neglected energy contributions from the local moments of defects, and $Fe_{Al}$ is special, in that this effect is probably sufficient to cancel approximately the energy contribution to $E_f$ from magnetism in bcc-Fe. It is likely that this defect has a large local moment, because its structure is in effect a nine-atom unit of bcc-Fe. If this is the case, then $E_f \approx 0$ eV in Fe-rich FeAl, rising to a few tenths of an electron volt when excess Al is present.

**Table 6.** Calculated formation energies $E_f$ (eV) for $B_{Al}$, $B_{Fe}$ and $B_i$ under Al-rich ($\mu_{Al} = \mu_{fcc\text{-}Al}$) and Fe-rich ($\mu_{Fe} = \mu_{bcc\text{-}Fe}$) conditions in $B2$-FeAl with respect to $\mu_B = \mu_{B(FeB)}$ and $\mu_B = \mu_{B(Fe_2B)}$ in supercells with 54 lattice sites. The state that gives the minimum level for $\mu_B$ and maximizes $E_f$ is taken to be the standard one (**bold**).

| | | Al-rich | | | Fe-rich | | |
|---|---|---|---|---|---|---|---|
| $\mu_B$ | Fe pseudo-potential | $B_{Al}$ | $B_{Fe}$ | $B_i$ | $B_{Al}$ | $B_{Fe}$ | $B_i$ |
| *All spin-averaged* | | | | | | | |
| FeB | Fe-TM-soft | **1.12** | **1.25** | **1.40** | 1.12 | 3.66 | 2.62 |
| FeB | Fe-TM-hard | **1.18** | **1.29** | **1.47** | 1.18 | 3.65 | 2.64 |
| $Fe_2B$ | Fe-TM-soft | 0.39 | 0.52 | 0.67 | **1.59** | **4.14** | **3.09** |
| $Fe_2B$ | Fe-TM-hard | 0.49 | 0.61 | 0.78 | **1.67** | **4.13** | **3.13** |
| *Spin-polarized bcc-Fe, FeB and $Fe_2B$* | | | | | | | |
| FeB | Fe-TM-soft | **1.25** | **1.38** | **1.53** | 1.25 | 2.80 | 2.24 |
| FeB | Fe-TM-hard | 1.51 | 1.63 | 1.80 | 1.51 | 1.92 | 1.95 |
| $Fe_2B$ | Fe-TM-soft | 0.74 | 0.87 | 1.03 | **1.45** | **3.00** | **2.44** |
| $Fe_2B$ | Fe-TM-hard | **1.67** | **1.79** | **1.96** | **1.82** | **2.23** | **2.25** |

### *3.4. Vacancy–antisite pairs*

Now we consider what happens when vacancies are combined with antisites in FeAl to create vacancy–antisite pairs. If a $V_{Al}$ defect is placed next to an $Al_{Fe}$ defect (in a supercell with 54 atomic sites and using the Fe-TM-soft pseudopotential), then the defect spontaneously rearranges itself so that the $Al_{Fe}$ atom moves into the vacancy, leaving behind a $V_{Fe}$ defect. In other words, the $V_{Al}$–$Al_{Fe}$ is completely unstable, and decomposes without any energy barrier into $V_{Fe}$. The energy for the reaction $V_{Al} + Al_{Fe} \rightarrow V_{Fe}$, where $V_{Al}$ and $Al_{Fe}$ are initially isolated, is about 3.48 eV. The outcome when $V_{Fe}$ is placed next to $Fe_{Al}$ is completely different. This forms a stable $V_{Fe}$–$Fe_{Al}$ complex that is about 0.10 eV lower in energy than the sum of its isolated components. Moreover, the reaction that would change this complex into $V_{Al}$ costs 1.64 eV; hence, $V_{Al}$ is only a metastable defect.

Thus, iron vacancies are stabilized by both forming pairs and combining with $Fe_{Al}$ antisite defects. In Al-rich material, $Fe_{Al}$ has a higher formation energy than the binding energy of $V_{Fe}$–$Fe_{Al}$ complexes, hence the complexes, although stable, would be relatively rare. The binding energy of the di-vacancy $(V_{Fe})_2$, on the other hand, being comparable within the accuracy of the method to $E_f$ for the monovacncy $V_{Fe}$, makes it likely that a significant population of both types of defect could exist. When the system contains excess Fe, we expect more $Fe_{Al}$ antisite defects to be present, and some Fe monovacancies may be trapped by them, effectively reducing $E_f$ for both types of defect. Also, the binding energy of $(V_{Fe})_2$ is now smaller than $E_f$ for $V_{Fe}$. Therefore, more monovacancies—either in the form of isolated defects or as $V_{Fe}$–$Fe_{Al}$ complexes—are likely to exist than $(V_{Fe})_2$ di-vacancies.

### *3.5. Boron in FeAl*

The formation energies for substitutional and interstitial boron calculated by the AIMPRO method are presented in table 6. In all cases, a supercell that has 54 atomic sites in pure $B2$-FeAl is used. The calculations are complicated by the existence of more than one phase for the source of boron to consider, namely FeB and $Fe_2B$. We take the standard value for $\mu_B$ to be the state where it is lowest. This makes $E_f$ largest. It can be seen from the table that both magnetism and pseudopotential affect the outcome. In all cases, when the system contains an excess of Fe, the formation energies of defects containing boron are higher relative to $Fe_2B$ than to FeB. Therefore, in Fe-rich conditions, $\mu_B$ is lowest in $Fe_2B$. When the system has excess Al, and only spin-averaged total energies are used, $E_f$ is largest with respect to FeB. Using spin-

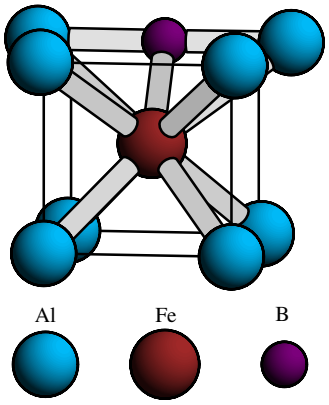


**Figure 4.** Structure of the interstitial boron defect in FeAl.
(This figure is in colour only in the electronic version)

polarized total energies for the reference chemical potentials with the 'soft' Fe pseudopotential does not change the ordering; however, $E_f$ for the defects is largest with respect to $Fe_2B$ with the 'hard' Fe pseudopotential.

In all conditions and all cases, $B_{Al}$ has the lowest formation energy of the three types of defect, and is minimum in Al-rich material. The Fe:Al stoichiometry has a large effect on the overall range of values for $E_f$. The three types of defect are closer in energy to one another in Al-rich FeAl than when there is excess Fe. Using spin-polarized total energies for the chemical potentials reduces the spread in energies for Fe-rich material. Of the three defects, $B_i$ has the most complicated structure; $B_{Al}$ and $B_{Fe}$ have very little structural relaxation associated with them. The minimum energy configuration for $B_i$ lies at the octahederal site midway between a pair of Al atoms: see figure 4. The two neighbouring Al atoms move away from their normal lattice sites 1.413 Å from the $B_i$ atom to a distance of 1.870 Å. The four equivalent next-nearest-neigbouring Fe atoms remain close to their normal lattice sites, and are located at a distance of 1.920 Å. The complementary octahederal site for $B_i$ is about 0.80 eV higher in energy.

In the previous section it was shown that $V_{Fe}$ is bound to $Fe_{Al}$ to form a stable complex $V_{Fe}$–$Fe_{Al}$. Its isolated constituents are also low-energy defects in the right conditions. Given that $B_{Al}$ has the lowest formation energy for isolated boron, two likely candidates for complexes containing boron are $V_{Fe}$–$B_{Al}$ and $Al_{Fe}$–$B_{Al}$. The first of these two complexes, $V_{Fe}$–$B_{Al}$, is found to be approximately 0.20 eV higher in energy than the sum of its isolated components; hence, it is a metastable defect, and not likely to exist in significant concentrations. The second complex $Al_{Fe}$–$B_{Al}$ is, on the other hand, found to be bound by 0.32 eV. Therefore, in Al-rich FeAl where the formation energy of $Al_{Fe}$ is minimum, boron can be trapped in the form of $Al_{Fe}$–$B_{Al}$ complexes, while in Fe-rich FeAl, isolated $B_{Al}$ will be the dominant form. Other complexes containing boron, while not entirely excluded, appear less likely to exist, due to having larger formation energies for the isolated components. These would require higher binding energies to stabilize them.

## 4. Summary and conclusions

We have used the AIMPRO *ab initio* pseudopotential method within the formalism of local density functional theory to model point defects and point defect complexes in $B2$-FeAl at the atomic

**Table 7.** Common defect types in Al-rich and Fe-rich FeAl.

| Stoichiometry | Constitutional defects | Vacancy types | Boron states |
|---|---|---|---|
| Al-rich | $Al_{Fe}$ | $V_{Fe}$, $(V_{Fe})_2$ | $B_{Al}$, $Al_{Fe}$–$B_{Al}$ |
| Fe-rich | $Fe_{Al}$ | $V_{Fe}$, $V_{Fe}$–$Fe_{Al}$ | $B_{Al}$ |

scale. While there is intentionally much overlap with earlier work, this study examines several other aspects of the problem, such as the effect of pseudopotential and basis construction and the choice of chemical potentials, in addition to providing alternative, newer values for the parameters reported. A summary of the main types of defects expected to exist in FeAl, based on the results of this work, is given in table 7.

In agreement with previous studies, the ideal, pure material is found to exhibit weak ferromagnetism. However, the contribution of spin-polarization being at most only 0.08 eV/FeAl is probably less than the accuracy with which formation energies can be calculated by the method. This is not true for the total energies of states that are strongly ferromagnetic and which act as chemical reservoirs for the formation of defects (i.e. bcc-Fe, FeB, and $Fe_2B$). Their potentials are significantly lower when magnetism is taken into account. The quality of the Fe pseudopotential also has a large effect on the total energies of these states, and hence the formation energies where they enter into the calculation. It is necessary to use an accurate description of the Fe3*d* electrons to obtain satisfactory results. This suggests that ultrasoft pseudopotential schemes (as used in [31–33]) can only produce meaningful results for states that do not involve magnetic contributions to the energy of a system from Fe3*d* electrons.

Of the native defects investigated, the Al-vacancy $V_{Al}$ is the least stable. Its formation energy is always too high for it to exist in significant concentrations. Moreover, the defect is unstable when combined with an $Al_{Fe}$ antisite defect, and transforms spontaneously into $V_{Fe}$ with an energy for the reaction of about 3.5 eV. These results also suggest that it will be necessary to find a new explanation for other positron annihilation experiments in which it is claimed that $V_{Al}$ has been observed in the form of $V_{Al}$–$V_{Fe}$ complexes [53]. The concentration of $V_{Al}$ is too small for $V_{Fe}$ to encounter it by diffusion, and $V_{Al}$ has such high energy that it seems unlikely that any partner will stabilize it. Conversely, the Fe vacancy $V_{Fe}$ is found to have a low formation energy in all conditions, in good agreement with experimental observations.

Experiments based on x-ray diffraction measurements of lattice parameter and density indicate that the vacancy formation energy decreases as Al content increases and, for $Fe_{0.502}Al_{0.498}$, $E_f = 0.51 \pm 0.07$ eV [54]. More recently, similar experiments, but with different assumptions in the analysis, obtain a nearly identical result where $E_f = 0.51 \pm 0.14$ eV for stoichiometric material [55]. However, in their conclusions, the authors caution that the difficulty of measuring the true composition, combined with the sensitivity of the formation energy to composition, means in fact that a more reasonable estimate is $E_f \approx 0.5$–$0.8$ eV. Nevertheless, these values compare favourably with our caculated energies $E_f \approx 0.4$–$0.6$ eV, in Al-rich and Fe-rich material, using the Fe-TM-hard pseudopotential, and spin-polarized, ferromagnetic bcc-Fe for $\mu_{Fe}$.

Notice that $E_f$ for $V_{Fe}$ is significantly overestimated in Fe-rich material when the Fe-TM-soft pseudopotential is used. The discrepancy is even larger, amounting to about $\approx$1 eV if magnetism in bcc-Fe is neglected. If this were the case, then Fe-rich FeAl would contain few vacancies, in clear contradiction with experimental observations.

The $V_{Fe}$ defect can lower its energy by binding to an $Fe_{Al}$ antisite to create a stable antisite–vacancy complex $V_{Fe}$–$Fe_{Al}$, or by combining with a second $V_{Fe}$ to create an iron

di-vacancy $(V_{Fe})_2$. In FeAl containing excess Fe where $Fe_{Al}$ antisite defects are expected to exist in relatively high concentrations, $V_{Fe}$–$Fe_{Al}$ complexes can form. When the material contains excess Al, the converse is true. Moreover, $E_f$ for $V_{Fe}$ changes from being about double the binding energy of $(V_{Fe})_2$ to nearly the same as the Al-content increases. Thus, our results suggest that the concentration of $(V_{Fe})_2$ will increase as the iron content decreases. This is consistent with the direct observation of vacancy-type defects in FeAl using positron annihilation experiments, where it is concluded that, in the $B2$ phase, positrons are trapped at sites with an open volume that is approximately double the size of a single vacancy, and that the concentration of these defects increases with increasing Al-content [56, 57]. The measured defect formation energy is estimated to be $E_f \approx 0.7$–1 eV, which is a value similar to that found in earlier experiments [58]. These energies can be interpreted as representing the energy to create a di-vacancy from two monovacancies minus their binding energy.

Although $V_{Al}$ has a formation energy that is too high for it to have a significant concentration in FeAl, the results imply that when defects are centered on an Al-site, such as $Fe_{Al}$ and $B_{Al}$, they might be sensitive to the choice of Fe pseudopotential. However, in these two cases the calculations show that the Fe pseudopotential has very little effect on $E_f$ either when spin-polarization is neglected or when atoms in ferromagnetic reservoirs are not involved. It has also been found that $E_f$ for $V_{Al}$ is ∼0.1–0.2 eV smaller in a large supercell with 128 atomic sites than in one with 54 atomic sites. The larger supercell allows greater freedom for the relaxation of the atoms surrounding a defect. Similar calculations for other open defects ($V_{Fe}$, $(V_{Fe})_2$) that might be overconstrained in a supercell with 54 atomic sites find that their energy is not significantly differerent when the larger-sized supercell is used, therefore $V_{Al}$ can probably be considered to be a 'worst case'.

The $Al_{Fe}$ antisite defect is found to have, in Al-rich conditions, essentially zero formation energy, thus it is the constitutional defect that accommodates excess aluminium. $V_{Fe}$ and $(V_{Fe})_2$, being low-energy defects, may also make a minor contribution here. The complementary case, $Fe_{Al}$ in Fe-rich FeAl, is complicated by the effects of magnetism. When spin-polarization is completely neglected for all states, its formation energy is nearly the complement of $Al_{Fe}$. However, when bcc-Fe is treated as being ferromagnetic, $\mu_{bcc\text{-}Fe}$ is much lower, which raises $E_f$ for $Fe_{Al}$ in Fe-rich FeAl substantially. The amount is greater with the Fe-TM-hard pseudopotential than the Fe-TM-soft pseudopotential. The structure of the defect is similar to that for a nine-atom unit of bcc-Fe; therefore, it is likely that this defect can lower its energy by having a relatively large local moment, which is not included in our calculations. It is reasonable to expect that the energy contribution from the defect's local moment is sufficient to make $E_f \approx 0$ eV. A further argument in favour of this is that the excess Fe must somehow be accommodated, and $V_{Al}$ is clearly excluded; $Fe_{Al}$ is the only suitable defect.

Isolated substitutional and interstitial boron has formation energies in the range ≈1.1–1.8 eV in Al-rich FeAl, while being generally higher in Fe-rich material. The lowest energy state in all conditions, $B_{Al}$, binds strongly with $Al_{Fe}$ to form stable $Al_{Fe}$–$B_{Al}$ complexes. These complexes will form when the system contains excess Fe, however they are predicted to be more common in Al-rich FeAl where $Al_{Fe}$ is expected to exist in relatively high concentrations. The solubility of B in Fe-rich FeAl is limited solely by the existence of $Fe_2B$, but is not limited when the system contains excess Al. Furthermore, the formation energy for $B_i$ is not particularly high in Al-rich FeAl and only slightly higher than for substitutional B, while in Fe-rich FeAl, $B_i$ is a high-energy defect. Diffusion of impurity atoms usually occurs via an interstitial form, which suggests that very little migration of boron will occur in FeAl with a high iron content.

The fact that $V_{Fe}$ and $V_{Fe}$–$Fe_{Al}$, together with $Fe_{Al}$, are defects with a low formation energy in Fe-rich FeAl provides support for the idea from experiments that vacancies play

an important role in the mechanical properties of the material. Antiphase boundaries can be viewed as a thin layer containing an array of antisite atoms that join two regions of crystal displaced by half of the lattice spacing in a given direction. It is possible to construct such layers with different arrangements and numbers of antisite atoms. Since the formation energy of antisite atoms depends strongly on the stoichiometry of the system, the structure and form of antisite boundaries are, by analogy, likely to be affected by local chemical potentials in a similar way. This will have further consequences, we expect, for the interactions of point defects with antiphase boundaries in a manner that resembles the properties of $V_{Fe}$–$Fe_{Al}$ and $Al_{Fe}$–$B_{Al}$ complexes. Similarly, structures that are related to these complexes in the vicinity of dislocation cores may also exist, thereby affecting the mechanical properties of the material. For example, when an extended defect encounters $V_{Fe}$ or $B_{Al}$ defects, it may create $V_{Fe}$–$Fe_{Al}$ or $Al_{Fe}$–$B_{Al}$ complexes in its wake. A more specific example concerns slip on cubic planes. Recall that, above the temperature at which the peak in yield stress occurs and where normal behaviour resumes, the predominant slip system consists of ⟨100⟩ dislocations. These dislocations glide on {100} planes, and consequently have either purely Al or Fe cores. Therefore, each type will encounter fundamentally different defects, i.e. $Fe_{Al}$ and $B_{Al}$ on Al planes, and $V_{Fe}$ on Fe planes. Thus, cubic dislocations with Fe cores can absorb vacancies and undergo climb, thereby moving to an Al plane, while the reverse is much less likely.

## Acknowledgments

The authors wish to thank Region Rhône-Alpes for financial support under contract number 815141 (Improvement of high temperature mechanical properties of iron-aluminium alloys). We also thank the EPSRC in the UK for providing supercomputing facilities for the e6 consortium. SÖ and CDL thank VR in Sweden for providing financial support and computer facilities. Finally, we thank Matti Alatalo (Lappeenranta) for helpful discussions.

## Appendix

FeB has four formula units (eight atoms) per unit cell, and $Fe_2B$ has two formula units (six atoms) per unit cell. The atomic coordinates in the unit cell for FeB are described by four parameters $A$, $B$, $C$, and $D$, while for $Fe_2B$ there is one parameter $A$. These parameters are defined by table A.1.

**Table A.1.** Atom positions for FeB and $Fe_2B$ expressed in fractional coordinates of the lattice parameters.

| Fe | | | B | | |
|---|---|---|---|---|---|
| $x$ | $y$ | $z$ | $x$ | $y$ | $z$ |
| FeB | | | | | |
| $0.0 + A$ | 0.25 | $0.0 + B$ | $0.0 + C$ | 0.25 | $0.0 + D$ |
| $0.0 - A$ | 0.75 | $0.0 - B$ | $0.0 - C$ | 0.75 | $0.0 - D$ |
| $0.5 - A$ | 0.75 | $0.5 + B$ | $0.5 - C$ | 0.75 | $-0.5 + D$ |
| $0.5 + A$ | 0.25 | $0.5 - B$ | $0.5 + C$ | 0.25 | $0.5 - D$ |
| $Fe_2B$ | | | | | |
| $0.5 + A$ | $0.0 + A$ | 0.25 | 0.0 | 0.0 | 0.0 |
| $1.0 - A$ | $0.5 + A$ | 0.25 | 0.0 | 0.0 | 0.5 |
| $0.5 - A$ | $1.0 - A$ | 0.25 | | | |
| $0.0 + A$ | $0.5 - A$ | 0.25 | | | |

## References


[1] Fraczkiewicz A, Gay A S and Biscondi M 1998 *Mater. Sci. Eng.* A **258** 108–14
[2] Calonne O, Fraczkiewicz A and Louchet F 2000 *Scr. Mater.* **43** 69–75
[3] Golovin I S, Neuhäuser H, Rivière A and Strahl A 2004 *Intermetallics* **12** 125–50
[4] George E P and Baker I 1998 *Phil. Mag.* A **77** 737–50
[5] George E P and Baker I 1998 *Intermetallics* **6** 759–63
[6] Baker I and Yang Y 1997 *Mater. Sci. Eng.* A **239/240** 109–17
[7] Jordan J L and Deevi S C 2003 *Intermetallics* **11** 507–28
[8] Yoshimi K, Hanada S and Yoo M H 1995 *Acta Metall. Mater.* **43** 4141–51
[9] Morris D G and Morris M A 1997 *Intermetallics* **5** 245–63
[10] Morris D G and Muñoz-Morris M A 2005 *Intermetallics* **13** 1269–74
[11] Zou J and Fu C L 1995 *Phys. Rev.* B **51** 2115–21
[12] Sundararajan V, Sahu B R, Kanhere D G, Panat P V and Das G P 1995 *J. Phys.: Condens. Matter* **7** 6019–34
[13] Bogner J, Steiner W, Reissner M, Mohn P, Blaha P, Schwarz K, Krachler R, Ipser H and Sepiol B 1998 *Phys. Rev.* B **58** 14922–33
[14] Kulikov N I, Postnikov A V, Borstel G and Braun J 1999 *Phys. Rev.* B **59** 6824–33
[15] Lechermann F, Welsch F, Elsässer C, Ederer C, Fähnle M, Sanchez J M and Meyer B 2002 *Phys. Rev.* B **65** 132104
[16] Wang C S, Klein B M and Krakauer H 1985 *Phys. Rev. Lett.* **54** 1852–5
[17] Asada T and Terakura K 1992 *Phys. Rev.* B **46** 13599–602
[18] Kong L T and Liu B X 2004 *Appl. Phys. Lett.* **84** 3627–9
[19] Mohn P, Persson C, Blaha P, Schwarz K, Novák P and Eschrig H 2001 *Phys. Rev. Lett.* **87** 196401
[20] Das G P, Rao B K, Jena P and Deevi S C 2002 *Phys. Rev.* B **66** 184203
[21] Petukhov A G, Mazin I I, Chioncel L and Lichtenstein A I 2003 *Phys. Rev.* B **67** 153106
[22] Anisimov V I, Aryasetiawan F and Lichtenstein A I 1997 *J. Phys.: Condens. Matter* **9** 767–808
[23] Arrott A and Sato H 1959 *Phys. Rev.* **114** 1420–6
[24] Sato H and Arrott A 1959 *Phys. Rev.* **114** 1427–40
[25] Reddy B V, Deevi S C, Reuse F A and Khanna S N 2001 *Phys. Rev.* B **64** 132408
[26] Smirnov A V, Shelton W A and Johnson D D 2005 *Phys. Rev.* B **71** 064408
[27] Fu C L, Ye Y Y, Yoo M H and Ho K M 1993 *Phys. Rev.* B **48** 6712–5
[28] Fu C L 1995 *Phys. Rev.* B **52** 3151–8
[29] Fu C L and Zou J 1996 *Acta Mater.* **44** 1471–8
[30] Medvedeva N I, Gornostyrev Y N, Novikov D L, Mryasov O N and Freeman A J 1998 *Acta Mater.* **46** 3433–42
[31] Fähnle M, Mayer J and Meyer B 1999 *Intermetallics* **7** 315–23
[32] Fähnle M, Meyer B, Bester G, Majer J and Börnsen N 2001 *Defects Diffus. Forum* **194–199** 279–85
[33] Besson R, Legris A and Morillo J 2002 *Phys. Rev. Lett.* **89** 225502
[34] Lechermann F, Fähnle M and Sanchez J M 2005 *Intermetallics* **13** 1096–109
[35] Briddon P R and Jones R 2000 *Phys. Status Solidi* b **217** 131–71
[36] Coutinho J, Jones R, Briddon P R and Öberg S 2000 *Phys. Rev.* B **62** 10824–40
[37] Perdew J P and Wang Y 1992 *Phys. Rev.* B **45** 13244–9
[38] Latham C D, Jones R, Öberg S and Briddon P R 2001 *Phys. Rev.* B **63** 155202
[39] Troullier N and Martins J L 1991 *Phys. Rev.* B **43** 1993–2006
[40] Louie S G, Froyen S and Cohen M L 1982 *Phys. Rev.* B **26** 1738–42
[41] Monkhorst H J and Pack J D 1976 *Phys. Rev.* B **13** 5188–92
[42] Zhang S B and Northrup J E 1991 *Phys. Rev. Lett.* **67** 2339–42
[43] Northrup J E and Zhang S B 1993 *Phys. Rev.* B **47** 6791–4
[44] Pöykkö S, Puska M J and Nieminen R M 1996 *Phys. Rev.* B **53** 3813–9
[45] Mattila T and Nieminen R M 1996 *Phys. Rev.* B **54** 16676–82
[46] Van de Walle C G, Limpijumnong S and Neugebauer J 2001 *Phys. Rev.* B **63** 245205
[47] Watson R E and Weinert M 1998 *Phys. Rev.* B **58** 5981–8
[48] Meschel S V and Kleppa O J 2001 *J. Alloys Compounds* **321** 183–200
[49] Colinet C 2003 *Intermetallics* **11** 1095–102
[50] Perkins R S and Brown P J 1974 *J. Phys. F: Met. Phys.* **4** 906–20
[51] Brown P J and Cox J L 1971 *Phil. Mag.* **23** 705–25
[52] Joyner D J, Johnson O, Hercules D M, Bullett D W and Weaver J H 1981 *Phys. Rev.* B **24** 3122–37
[53] Haraguchi T, Horib F, Oshimab R and Kogachi M 2001 *Intermetallics* **9** 763–70
[54] Kogachi M and Haraguchi T 1997 *Mater. Sci. Eng.* A **230** 124–131
[55] Schneibel J H and Pike L M 2004 *Intermetallics* **12** 85–90

[56] Broska A, Wolff J, Franz M and Hehenkamp T 1999 *Intermetallics* **7** 259–67
[57] Wolff J, Franz M, Broska A, Kerl R, Weinhagen M, Köhler B, Brauer M, Faupel F and Hehenkamp T 1999 *Intermetallics* **7** 289–300
[58] Würschum R, Grupp C and Schaefer H E 1995 *Phys. Rev. Lett.* **75** 97–100